Energy Conversion and Management 148 (2017) 1082–1095

Contents lists available at ScienceDirect

Energy Conversion and Management

journal homepage: www.elsevier.com/locate/enconman

Heat transfer and pressure drop characteristics of R134a flow boiling in the parallel/tandem microchannel heat sinks

Yaxian Zhang [1], Jingtao Wang [1], Wei Liu, Zhichun Liu *

School of Energy and Power Engineering, Huazhong University of Science and Technology, Wuhan 430074, China

ARTICLE INFO

Article history:
Received 21 March 2017
Received in revised form 29 May 2017
Accepted 20 June 2017
Available online 1 July 2017

Keywords:
Microchannel heat sinks
Multi-heat sources
Parallel
Series
Experiment

ABSTRACT

With the rapid development of integrated electronic devices, microchannel heat sinks cooling system containing two heat sinks in parallel or in series has been established, for the purpose of meeting the demand of removing high heat fluxes from multi-heat sources in small space. Using refrigerant R134a as working fluid, the flow boiling characteristics of R134a and the mutual influences between the microchannel heat sinks were investigated experimentally under dynamic and stable conditions to evaluate the feasibility of this cooling system applied to engineering. The heat sinks were connected in parallel or in series, each of them consisting of 21 microchannels with hydraulic diameter of 0.5 mm. For heat sinks in parallel, pressure drop of the heat sink in subcooled boiling changed and eventually resulted in uneven mass flux distribution, where flow rate of the heat sink became less than 0.4 L/min and the total volume flow rate stabilized at 0.8 L/min. Correlations for heat transfer coefficients and friction factors of single heat sink in single-phase convective flow and subcooled flow boiling were proposed, providing acceptable predictions with mean absolute errors less than 8%. Based on the correlations, a steady-state mathematical model was established to describe the steady-state characteristics of parallel microchannel heat sinks. For heat sinks in series, temperature of upstream heat sink remained constant except for the moment phase change occurred in downstream heat sink with outlet and wall temperature of the upstream one jumping by 0.5 °C and 0.1 °C respectively. The results indicated that downstream effects on the upstream were weak. But phase transition of upstream heat sink affected heat transfer of downstream heat sink more intensely, with inlet, outlet and wall temperature of the downstream one decreasing by 2.5 °C. The cooling system proposed has the advantages of compact structure, simple connection, cost-saving, easy-maintenance and reliable operation. The experimental results have guiding significance for solving heat dissipation problem of high heat flux electronic devices with multi-heat sources.

1. Introduction

The heat flux of microelectronic devices has increased substantially, from 10 W/cm^2 in the 1970s rising to 10^2 W/cm^2 in the 1990s. At present the heat consumption of Intel Core i7 Processor Extreme Edition Series has grown up to 10 W/cm^2, let alone the servers with multiple processors. Due to the stability and reliability of electronic devices are facing severe challenges caused by the rise of operating temperatures, it's urgent to utilize efficient and reliable cooling technology for solving the above problems.

Several related solutions have been proposed in recent years. Tuckerman and Pease [1] pioneered the concept of heat sink in 1981. Through two aspects of theory and experiments, they verified that the heat transfer coefficient would be significantly increased for laminar flow in micro-scale channels, and inversely proportional to the equivalent size of the channel.

The microchannel heat sink cooling system presents some remarkable advantages such as compact structure and excellent heat transfer performance, and it has become one of the most potential and highly efficient cooling equipment. Shen et al. [2] took the effects of surface roughness on flow and heat transfer in microchannels into consideration. It had a strong impact on laminar flow except for low Reynolds number. Yun et al. [3] measured the heat transfer and flow characteristics of R410A in rectangular microchannels with hydraulic diameters of 1.36 and 1.44 mm at various test conditions. They found the boiling heat transfer coefficients of R410a in microchannels were much higher than those in large diameter tubes. Based on experiments using R134a flowing in a horizontal tube with inner diameter of 2 mm, Yan and Lin [4]

* Corresponding author at: 1037 Luoyu Road, Hongshan District, Wuhan 430074, China.
E-mail address: zcliu@hust.edu.cn (Z. Liu).
[1] Y.X. Zhang and J.T. Wang contributed equally to this work.

http://dx.doi.org/10.1016/j.enconman.2017.06.067
0196-8904/

Nomenclature

A	area [cm^2]
G	volume flux [L/min]
T	temperature [K]
ΔT	degree of wall superheat [K]
h	heat transfer coefficient [W/m^2 K]
q'	heat flux [W/cm^2]
i	specific enthalpy [J/kg]
ΔP	pressure drop [Pa]
g	gravitational acceleration [m/s^2]
h_f	frictional heat loss [m]
h_j	local head loss [m]
v	velocity [m/s]
Nu	Nusselt number
Pr	Prandtl number
Re	Reynolds number
D	hydraulic diameter [m]
MAE	mean absolute error
f	flow resistance coefficient
Q_r	relative heat flux

Greek symbols

Δ	gradient [–]
ρ	density [kg/m^3]
λ_f	friction factor
λ	thermal conductivity [W/m K]
μ	dynamic viscosity [kg/m · s]
ν	kinematic viscosity [m^2/s]
α	thermal diffusivity [m^2/s]

Subscripts

sat	saturation
in	inlet
out	outlet
l	liquid
v	vapor
cor	correlation
exp	experiment
fluid	fluid
wall	wall
heated	heated
A	heat sink A
B	heat sink B
sub	subcooled flow boiling
con	convective flow

investigated the effects of imposed wall heat flux, mass flux, vapor quality and saturation temperature. They noted that the evaporation heat transfer coefficient for small tubes was 30–80% more than that for larger tubes. The experiments for R134a flowing in horizontal small-diameter tubes with inner diameter of 0.51, 1.12 and 3.1 mm, from Saitoh et al. [5] showed at lower vapor quality, the local heat transfer coefficient and the effect of mass flux on that decreased with decreasing tube diameter. Qu and Mudawar [6] obtained new data of critical heat flux (CHF) for flow boiling in a two-phase microchannel heat sink, They found that CHF in microchannel heat sinks was proportional to mass flux but independent of inlet temperature, and the previous correlations for single mini-channels were unsuitable for microchannel heat sinks. The experiments were conducted by Lie et al. [7] to investigated the heat transfer characteristics of R134a and R407C in horizontal small tubes. The results showed the evaporation heat transfer coefficients depended linearly on the vapor quality, except at low mass flux and high heat flux. Madhour et al. [8] measured local heat transfer coefficients of R134a flowing inside a multimicrochannel system at 35 locations, using a novel design of the test section and heater. The study was mainly aiming for energy-efficient microelectronic CPU cooling applications. do Nascimento et al. [9] evaluated the thermal performance of R134a flowing boiling in a microchannel-based heat sink. The results showed the highest heat sink averaged heat transfer coefficient based on the heated area was up to 36 kW/m^2 °C. As for static and dynamic flow instability of microchannel heat sink, Xu et al. [10] measured the onset temperature of flow instability was 93–96 °C, which was lower than the saturated temperature of 100 °C. In a very recent study, Thiangtham et al. [11] explained the effects of mass flux, heat flux, saturation temperature and vapor quality on the flow and heat transfer characteristics of R134a in a multi-microchannel heat sink.

Despite heat transfer and flow characteristics in microchannels have been extensively reported, studies about the mechanisms of flow boiling and the changes of flow patterns are not satisfactory enough. The experiments were performed in a small circular/rectangular channel with R12 by Tran et al. [12]. They noted that at all but the lowest wall superheats, heat transfer depended on heat flux, where nucleation mechanism dominated. At very low wall superheats, the heat transfer was strongly related to mass flux, where convective evaporation dominated. Owhaib et al. [13] presented an experimental investigation on saturated flow boiling of R134a in microchannels. Heat transfer coefficients were affected mainly by the wall heat flux and system pressure, but independent on mass flux and vapor quality, indicating that nucleate boiling is the dominant mechanism. Bao et al. [14] drew the same conclusions as above, by measuring the flow boiling heat transfer coefficients for R11 and HCFC123 in narrow passages. The two-phase flow patterns under boiling conditions in a microchannel heat sink were visualized by Chang and Pan [15]. The flow patterns were significantly different under stable or unstable conditions. Dong et al. [16] reported flow boiling of R134a in rectangular microchannel heat sinks. The results indicated for high heat flux cases, the thin film convective boiling determined the mean heat transfer coefficients, while for low heat flux cases, the nucleate boiling played a leading role. Bigham and Moghaddam [17] obtained synchronized images of bubbles from the experiments on flow boiling of FC-72 in a microchannel. As a bubble grew and flowed through the channel, four mechanisms of heat transfer were microlayer evaporation, interline evaporation, transient conduction and micro-convection, respectively. Through studying the heat transfer of saturated flow boiling for a new refrigerant R1233zd(E) in a multi-microchannel evaporator, Huang et al. [18] compared the data with correlations and came to a conclusion that the heat transfer mechanism dominating flow boiling was the thin liquid film evaporation. For space applications, Lee and Mudawar [19] explored the two-phase heat transfer mechanisms of large micro-channel evaporators using R134a. They classified dominant mechanisms at different quality ranges. Recently Markal et al. [20] investigated saturated flow boiling of deionized water in parallel microchannels by visualization method, and they noted that convective flow boiling was the key factor for flow boiling instabilities and underlying physical mechanisms of heat transfer in microchannels.

The ultimate goal of researching microchannel heat sinks is to design compact and efficient heat exchangers for the applications of cooling electronic devices. Many scholars have tried to change

the structures of microchannel heat sinks to meet these requirements. Mauro et al. [21] measured saturated critical heat flux in a microchannel cooper heat sink using three HFC refrigerants: R134a, R236fa and R245fa. Comparing split flow system (one inlet-two outlets) with single inlet/outlet system, they found the former system provided higher CHF and a much lower two-phase pressure drop. A double-layered silica microchannel heat sink with counter-flow arrangement was presented by Wu et al. [22], for the purpose of reducing thermal resistance and uniformizing the temperature distribution on the base surface of heat sink. Deng et al. [23] proposed a porous heat sink with reentrant microchannels fabricated by sintered cooper powder. Furthermore, Deng et al. [24] compared flow boiling characteristics of reentrant cooper microchannels with that of conventional rectangular microchannels. The results presented that heat transfer performance of the reentrant shapes was more enhanced. Dehghan et al. [25] found the heat transfer enhancement of micro-scale heat exchangers could be achieved by inserting rarefied porous inserts, especially in the slip-flow regime. The experiments were conducted to compare pool boiling heat transfer of porous interconnected microchannel nets (PIMN) with that of solid cooer interconnected microchannel nets (SIMN) by Zhang et al. [26]. The results indicated that PIMN suppressed the temperature excursion and exhibited a higher heat transfer coefficient. Xia et al. [27] reported that heat sink with corrugation microchannels provided better comprehensive performance compared with the conventional rectangular microchannel heat sink. Law et al. [28] demonstrated the benefits of oblique-finned microchannels with secondary microchannels in two-phase flow boiling mode. The inlet pressure fluctuations were significantly reduced by the stabilizing effects of oblique fins. The next year Law and Lee [29] performed a comparative study between straight-finned and oblique-finned microchannels with similar geometric parameters. The oblique structure yielded augmentations of 1.2–6.2 times in heat transfer coefficients and increments of 2.5–2.8 times in CHF values.

The studies for microchannel heat sinks have been proposed extensively, but all of them only take the condition of cooling single heat source into consideration. As a matter of fact, multi-heat sources have been widely applied in engineering projects, such as the server with multiple CPUs. Each CPU of the server requires a heat sink for cooling, and the heat sink works only when it's equipped with a complete cooling system. If meeting the above requirements, the whole heat sink system will not be compact, economical and reliable anymore. Therefore, how to dissipate heat from multi-heat sources efficiently by microchannel heat sinks is an increasing urgent problem to be solved.

In the present study, an accessible method of connecting two microchannel heat sinks in series or in parallel was proposed, while the heat sinks sharing a circulation system. The heat transfer and flow performance of microchannel cooling system in different connection modes was studied experimentally. In addition, the mutual influence between microchannel heat sinks was investigated from both dynamic and stable aspects. To the best of author's knowledge, the proposed construction composed of parallel or tandem heat sinks has scarcely been reported, with considerable importance of removing high heat flux for multi-heat sources.

2. Experimental system

2.1. Experimental apparatus and flow loop

Fig. 1 shows a schematic of the microchannel heat sinks cooling system applied in the experiment. All the components are marked with serial numbers in diagram. The system consisted of two subsystems, flow circulation system and data acquisition system.

The main components of the former system were gear pump, pre-heater, pressure protector, microchannel heat sinks, sight glass, condenser, manostat, dry filter, temperature controller, etc. They were connected by pipes and valves. The condenser used was a Danfoss brazed plate heat exchanger, and the type of gear pump was MG317XK/DC24W magnetic gear pump. The manostat was connected to the system pipeline by three-way valves, playing an important role in storing excess refrigerant and adjusting system pressure. As shown in Fig. 2, the main structure of manostat was reservoir chamber, placed in constant temperature water bath, to ensure the stability of system pressure.

In data acquisition system, the temperature was measured by K-type thermocouples with an uncertainty of $\pm 0.2\ ^{\circ}C$. To measure system pressure and pressure drop between the inlet and outlet of the test section, an absolute pressure sensors and a differential pressure transmitter from Yokogawa EJA110A series were selected. The mass flow rate was measured by a turbine flow meter known as model LWGY-6 with an accuracy grade of 0.5, ranging from 1.67 L/min to 10 L/min. The input power of heat source could be directly obtained by external power meter with the accuracy level of 0.5. The data mentioned above were input to the Keithley-2700 data acquisition instrument for recording and storage.

For a complete flow circulation in the experimental system, the refrigerant is driven by gear pump and heated to a specific temperature by pre-heater. Then refrigerant evaporates after flowing through the heat source and condenses into liquid in the plate heat exchanger. Being treated by dry filter afterwards, the working fluid will enter the next loop. What's more, the specific form of fluid can be observed through the sight glass.

2.2. Test section

According to the shape of the micro-fins, microchannel heat sink can be classified as rectangular, trapezoidal, triangular, etc.; according to the arrangement of microchannels, it can be divided into straight arrangement, staggered arrangement and so on. The depth and width of microchannels also have significant influence on heat transfer and flow condition. However, this paper mainly focused on the impact of different connection modes on the microchannel heat sink performance. Thus the structure of heat sink was not expected to be complicated. It was more appropriate to choose heat sink with rectangular ribs and simplified arrangement, as Fig. 3 shows.

The heat sink was fabricated in copper, with the overall height of 12 mm, length of 71 mm and width of 51 mm. It contains 21 channels with the cross section of $1.5 \times 1.5\ mm^2$ and channels are separated by ribs of 0.5 mm width. Two parts of microchannels are both 18 mm long in the flow direction.

As displayed in Fig. 3(c), the stainless steel bearing columns were installed on the baseplate of heat sink, with the purpose of enhancing disturbance, increasing loading capacity and preventing the heat sink surface from deformation under high-pressure operation. Taking into consideration the microchannel heat sink and heat source were bolted together, a 4 mm high lug boss was machined on the heat sink substrate with a heat transfer area ($45 \times 45\ mm^2$). In Fig. 4, there were 8 holes on the lug boss with an inner diameter of 2 mm, used for inserting the thermocouples to measure the temperature of heat sink bottom surface, inlet and outlet fluid. These thermocouples were sealed with thermal insulation adhesive. Due to the limitation of machining technology, the insertions of thermocouples were not deep enough to measure the center temperature of heat sink. However, by analyzing the thermal uniformity of heat sink, it was found that the maximum deviation between the temperature of measuring points and the

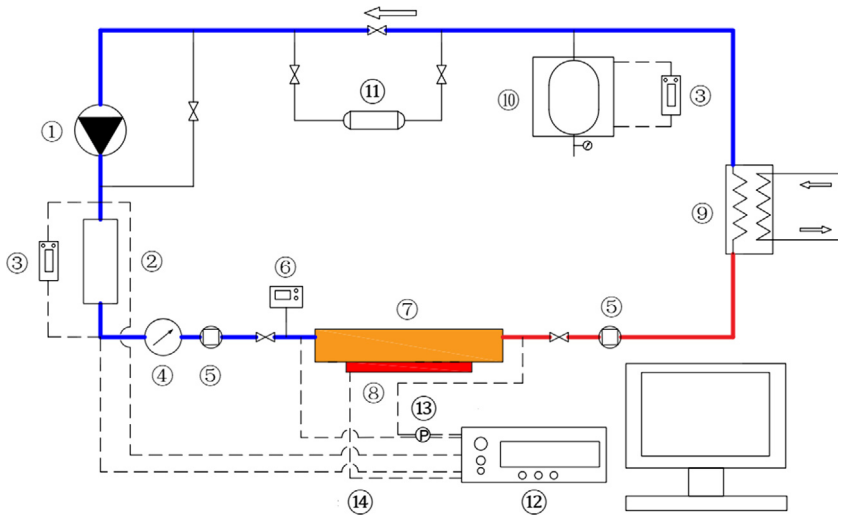

1. Gear pump
2. Pre-heater
3. Temperature controller
4. Flow meter
5. Sight glass
6. Pressure protector
7. Microchannel heat sink
8. Heat source
9. Condenser
10. Manostat
11. Dry filter
12. Data acquisition instrument
13. Pressure signal
14. Temperature signal

Fig. 1. Schematic diagram of the microchannel heat sinks cooling system.

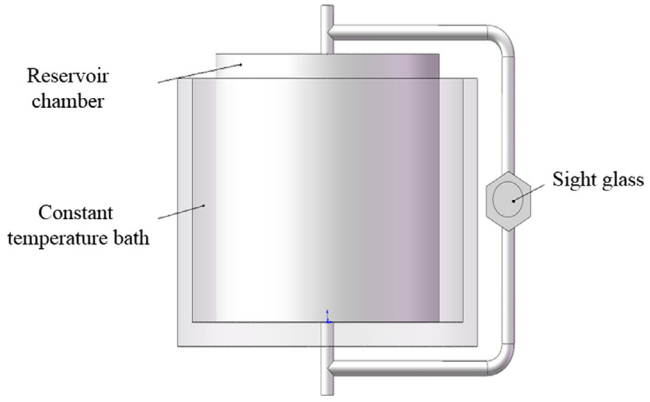

Fig. 2. Design diagram of manostat.

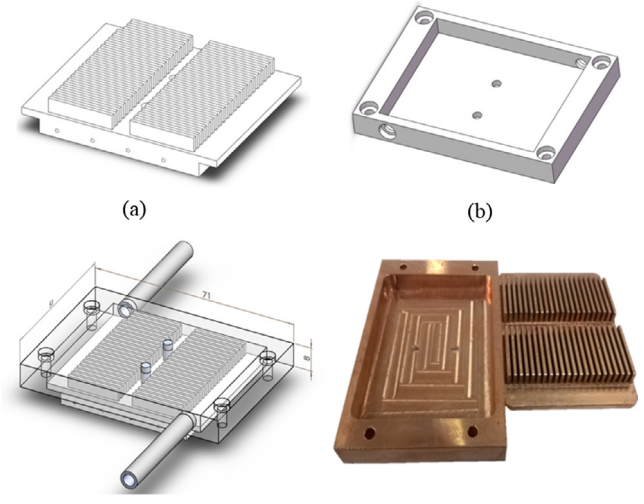

Fig. 3. Details of test section: (a) baseplate; (b) cover plate; (c) the overall diagram of microchannel heat sink and (d) product photo show.

mean temperature of bottom surface was less than 1.2 °C, which could support the reliability of measurement results.

In order to optimize the mass flux distribution in the microchannel heat sink, two stainless steel tubes with an inside diameter of 4 mm, outside diameter of 6 mm and length of 4 mm were welded to the inlet and outlet of heat sink, respectively. So that coolant can flow into the side inlet and out from the side outlet. The simulation result of the coolant flowing in the microchannel heat sink without heat transfer is shown in Fig. 5. The flow velocity distribution can be considered uniform, because the maximum deviation from average velocity was 9.7%. Although there was a small dead zone in the non-heat transfer section at each end, it had little effect on the heat transfer. And once the flow boiling occurs in microchannels, the mutual interference exists between gas-liquid two phases, which can improve flow uniformity to some extent.

2.3. Experimental heat sinks model in parallel/series

Microchannel heat sinks cooling system with multi-heat sources was established to investigate the mutual influences between heat sinks connected in parallel or in series, and R134a

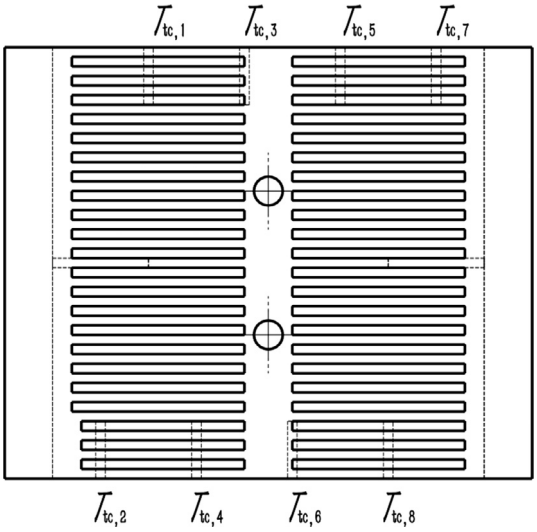

Fig. 4. Arrangement of the thermocouples.

was taken as working medium due to its advantages of safety, non-toxicity, environment-friendly and strong capability of heat exchange.

In the experimental models, two microchannel heat sinks were placed on the same horizontal plane and heated by two heat sources respectively. Fig. 6 shows the schematic of two heat sinks (A and B) in parallel connection. Taking the heat sink A as benchmark, the mutual influences were investigated when heat sink A in single-phase flow and subcooled boiling respectively, and gradually increasing the heating power of heat sink B. Part of the experimental parameters are displayed in Table 1.

Fig. 7 displays the diagram of two heat sinks (A and B) in series connection. From one hand, based on heat sink A, the influences on system performance were tested under the condition of heat sink A in the single-phase state, and the heating power of heat sink B gradually growing. From the other hand, under the circumstances of heat sink B in single-phase flow and subcooled boiling, the mutual influences were studied when gradually loading the heating power of heat sink A. Some test parameters adopted in the experiments are shown in Table 2.

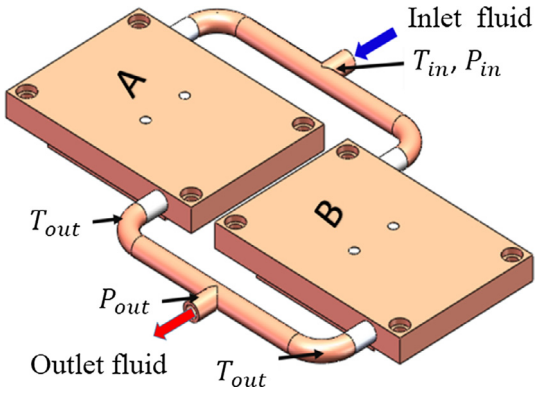

Fig. 6. Model of two micro-channel heat sinks in parallel connection.

Table 1
Test parameters in parallel connection.

G	T_{in}	T_{sat}
0.8 L/min	10 °C	20 °C

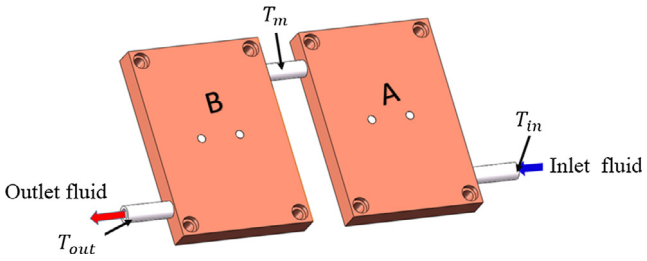

Fig. 7. Model of two micro-channel heat sinks in series connection.

Table 2
Test parameters in series connection.

G	T_{in}	T_{sat}
0.4 L/min	10 °C	20 °C

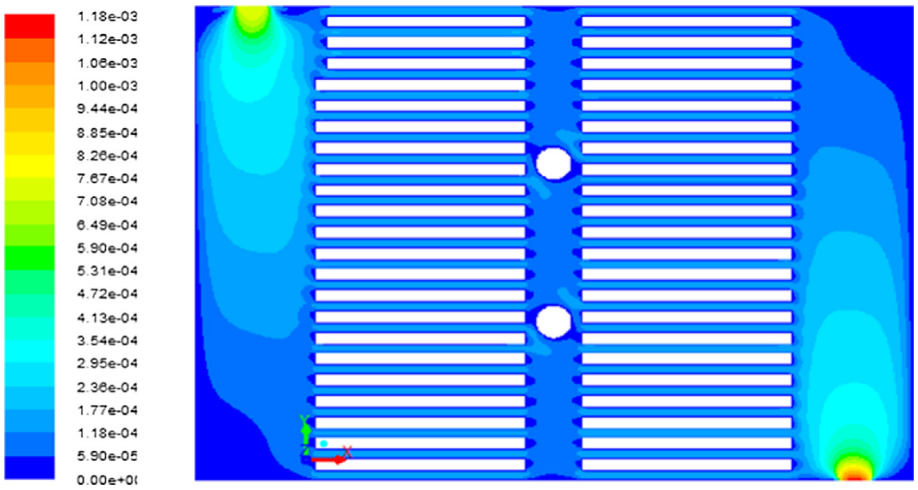

Fig. 5. Flow velocity distribution in the microchannel heat sink.

3. Data reduction

3.1. Experimental data processing

The tests were conducted under steady state and dynamic conditions. The parameters used to judge the performance of system were obtained from the experimental data.

For a given test, we assumed the heat flux added to the test section was distributed evenly, and ignored the thermal resistance of the heat sinks. The local heat transfer coefficient h of microchannel heat sink was determined by the following formula:

$$h = \frac{q'}{T_{wall} - T_{fluid}} \tag{1}$$

where T_{wall} is the mean temperature of heated surface, T_{fluid} is the average fluid temperature inside heat sink, and q' is the wall heat flux to the fluid.

The super-heated degree of heat sink wall was defined as:

$$\Delta T = T_{wall} - T_{sat} \tag{2}$$

where T_{sat} is the saturation temperature corresponding to the local pressure of working fluid R134a. All the thermal properties for R134a, including viscosity, density, enthalpy and thermal conductivity are acquired from the software REFPROP 9.0 developed by the National Institute of Standard and Technology (NIST).

Since the system pressure measuring points were located from the heat sink inlet and outlet a certain distance, the pressure drop in the pipeline would affect the calculation results and should be taken into consideration. The pipe pressure drop was computed from the following equation:

$$\Delta P = \rho g(h_f + h_j) \tag{3}$$

where h_j is the local head loss, selected according to the shape of pipeline; h_f is the frictional head loss and calculated as

$$h_f = \lambda_f \frac{l}{d} \frac{v^2}{2g} \tag{4}$$

where λ_f is the friction factor.

The experimental errors mainly included the calculated power error caused by heat dissipation of microchannel heat sinks, the pressure measurement error caused by pressure loss in pipeline, and the temperature measurement error caused by thermal resistance of pipeline and heat sinks. By means of error analysis, the heat loss of microchannel heat sinks was about 3%, while the maximum uncertainty of total heat transfer coefficient and mass quality was less than 15%.

It should be noted that the thermal contact resistance between heat sink and heat source was neglected in calculation process. Three reasons accounting for this are as follows. Initially heat sink and the heat source were tightly mounted with fixtures and connected by thermal grease, thus the thermal contact resistance between them was quite small. Furthermore, in practical applications the main concern is whether the temperature of heat source surface is within safe range. Additionally, the experimental measurement of thermal contact resistance of heat sink and heat source was complicated and it will be taken precisely to meet the needs of establishing an accurate theoretical model.

3.2. Correlation equations

Based on experimental researches, many correlation equations for predicting the heat transfer and flow resistance performance of microchannel heat sinks have been proposed. However, the flow conditions in microchannels are extremely complex and unstable because of the mal-distribution and phase-change of the working fluid. It should be mentioned that the applicable conditions for each correlation are limited. And it is necessary to propose new correlation equations available for the heat transfer coefficient and friction factor of these experiments.

The data were obtained from the experiments of microchannel single heat sink, divided into two parts of single-phase convective flow and subcooled boiling. The correlations were developed by introducing non-dimensional parameters of Nu, Pr and Re because the present data showed strong dependency on these parameters. By the means of least-squares estimation [30], the empirical correlations for the two conditions were obtained based on the present data.

3.2.1. Correlations for the heat transfer coefficient and friction factor in single-phase convective flow

The heat transfer coefficient h is defined as

$$h = \frac{\lambda}{D} Nu \tag{5}$$

where λ is the thermal conductivity of working fluid, D is the hydraulic diameter of microchannels.

The Nusselt number Nu is obtained from the present data, as shown in Eq. (6).

$$Nu = 6.0 Re^{0.59} Pr^{-2.17} \tag{6}$$

where two non-dimensional parameters are included in the above correlation, the Reynolds number Re and Prandtl number Pr. They are defined as

$$Re = \frac{\rho v D}{\mu} \tag{7}$$

$$Pr = \frac{v}{\alpha} \tag{8}$$

where μ is the dynamic viscosity, v is the kinematic viscosity and α is the thermal diffusivity.

It should be mentioned that the error of 25% was chosen as the criterion for assessing the fitting degree of empirical correlations and actual results, which is acceptable in engineering applications. Fig. 8 compares the experimental values of Nu with the predictions using the correlation. It shows that more than 95% of the predictions fall within ±25% of the experimental values. The mean absolute error MAE is 6%, defined as

$$MAE = \frac{1}{n} \sum \left(\left| \frac{Nu_{cor} - Nu_{\exp}}{Nu_{\exp}} \right| \right) \times 100\% \tag{9}$$

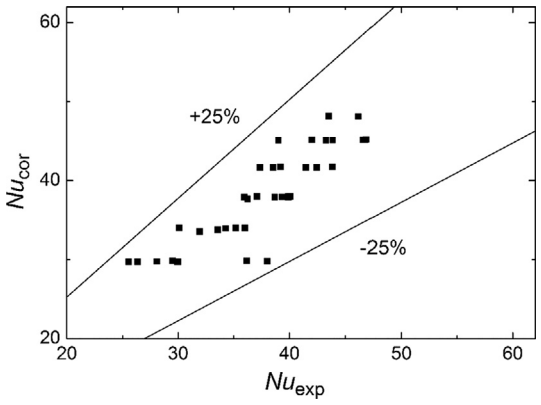

Fig. 8. Comparison of the experimental data with the predictive Nu by the correlation for single phase flow.

By analyzing the experimental data, the empirical formula of the flow resistance coefficient f in the microchannels is as follows.

$$f = 5.53Re^{-0.39} \quad (10)$$

Fig. 9 shows the comparison of the measured pressure drop loss with the predictions using the correlation. All the predictions fall within ±25% of the measured data. The mean absolute error *MAE* is 2%.

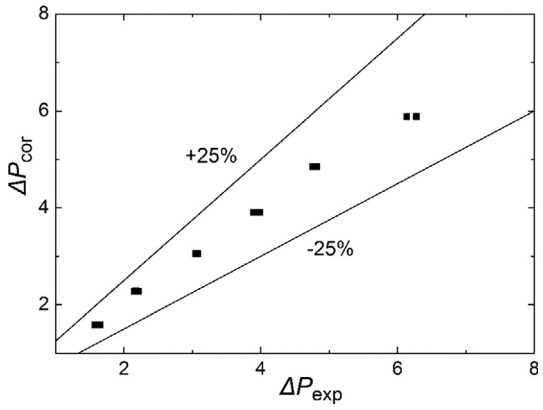

Fig. 9. Comparison of the measured pressure drop loss with the predictions for single phase flow.

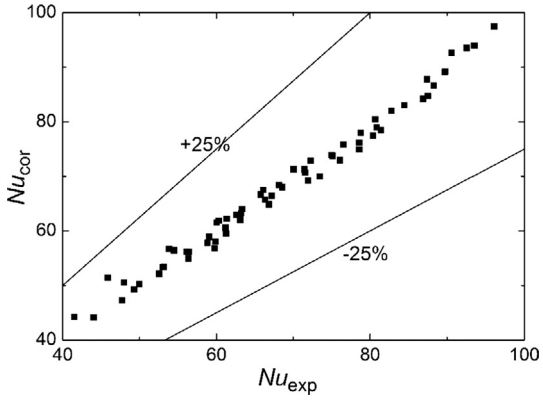

Fig. 10. Comparison of the experimental data with the predictive *Nu* by the correlation for subcooled flow boiling.

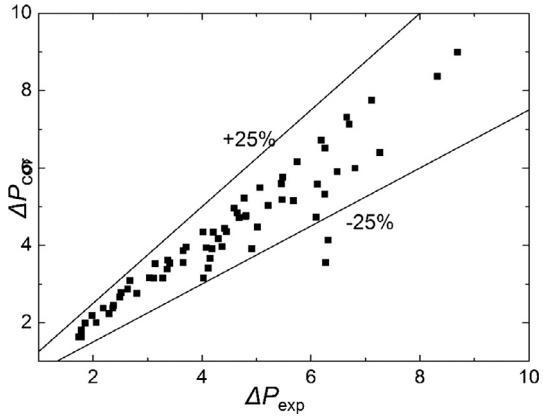

Fig. 11. Comparison of the measured pressure drop loss with the predictions for subcooled flow boiling.

3.2.2. Correlations for the heat transfer coefficient and friction factor in subcooled flow boiling

During the process of subcooled boiling, the heat flux has a great influence on the heat transfer coefficient. The relative heat flux *Qr* is used to describe this influence.

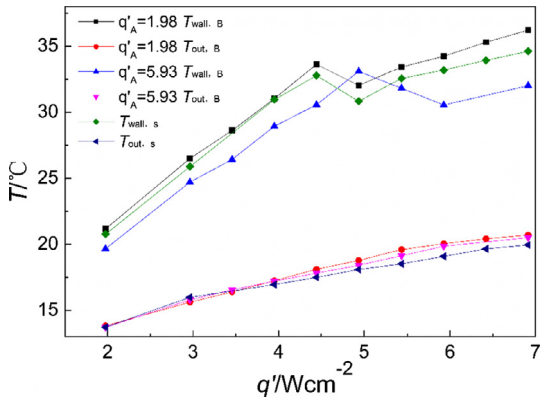

Fig. 12. Comparisons of parallel heat sinks with the single heat sink in terms of steady-state performance.

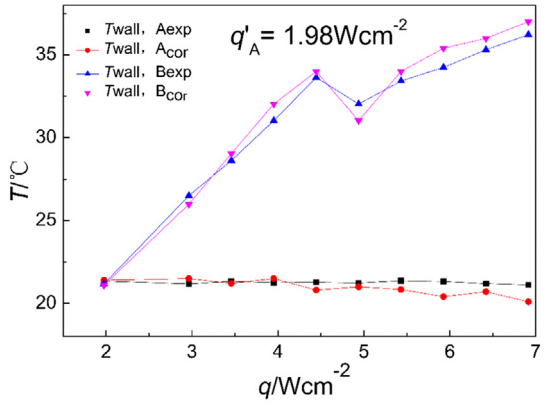

(a)

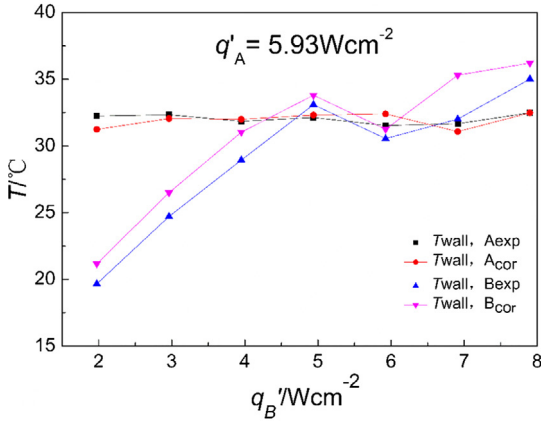

(b)

Fig. 13. Comparison of the measured bottom surface temperature of heat sinks A, B ($T_{wall,A}$, $T_{wall,B}$) with those predicted from proposed correlations, for two different heat fluxes of heat sink A: (a) 1.98 W/cm^2; (b) 5.93 W/cm^2.

$$Qr = \frac{q' A_{heated}}{\dot{m}(i_{(l,sat)} - i_{(l,in)})} \tag{11}$$

where $i_{(l,sat)}$ and $i_{(l,in)}$ are the specific enthalpy of saturated working fluid and inlet liquid, respectively.

"The mechanism of subcooled flow boiling has not yet reached an acknowledged conclusion and is influenced by complex factors. By introducing non-dimensional parameters of *Qr*, *Pr* and *Re*, the factors that are the comparison of imposed heat and latent heat, the physical parameters of working fluid, and the geometrical characteristics of microchannels have been taken into consideration, respectively. Based on the present data, the correlations for Nusselt number *Nu* and the flow resistance coefficient *f* are determined as Eqs. (12) and (13)."

$$Nu = 96.98 Re^{0.62} Pr^{-2.60} Qr^{0.72} \tag{12}$$

As shown in Fig. 10, more than 90% of the predictive data is within ±25% of the experimental values. The mean absolute error *MAE* is 2.1%.

In order to compare the measured pressure drop loss with the data predicted by the correlation, the flow resistance coefficient *f* in the microchannels is obtained as

$$f = 386.45 Re^{-0.37} Pr^{-0.90} Qr^{1.12} \tag{13}$$

The comparative result in Fig. 11 shows that more than 90% of the predictions fall within ±25% the measured data. The mean absolute error is 8%.

4. Results and discussion

4.1. Experimental results of heat sinks in parallel

In order to test the steady-state performance of parallel heat sinks, Fig. 12 presents the variations of bottom surface temperature and outlet temperature of heat sink B with imposed heat flux, for two different imposed heat fluxes of heat sink A, 1.98 W/cm^2 and 5.93 W/cm^2 respectively, at G = 0.8 L/min. The effects of imposed heat flux on single heat sink with G = 0.4 L/min are also examined and compared with heat sink B, as Fig. 12 shows.

Under the condition that heat sink A is in single-phase convective heat transfer ($q'_A = 1.98$ W/cm^2), heat sink B is in the same state when the heat flux is low, and the volume flow rate stabilizes at 0.4 L/min. The difference of pressure drop and temperature between heat sink B and the single heat sink is small. With the increase of heat flux, the refrigerant in heat sink B begins to vaporize, and transforms into subcooled boiling. The initial phase transition point is similar to the single heat sink. The bubbles generated in the microchannels leads to higher flow resistance in heat sink B. Then uneven flux distribution occurs between heat sink A and B, while the flow rate of heat sink B becomes less than 0.4 L/min. The temperature of bottom surface and outlet in heat sink B is gradually higher than that in the single heat sink at the same condition. Moreover, at higher heat flux the vaporization amount and flow resistance in heat sink B are much more increased, and the flow rate is further deviated from 0.4 L/min.

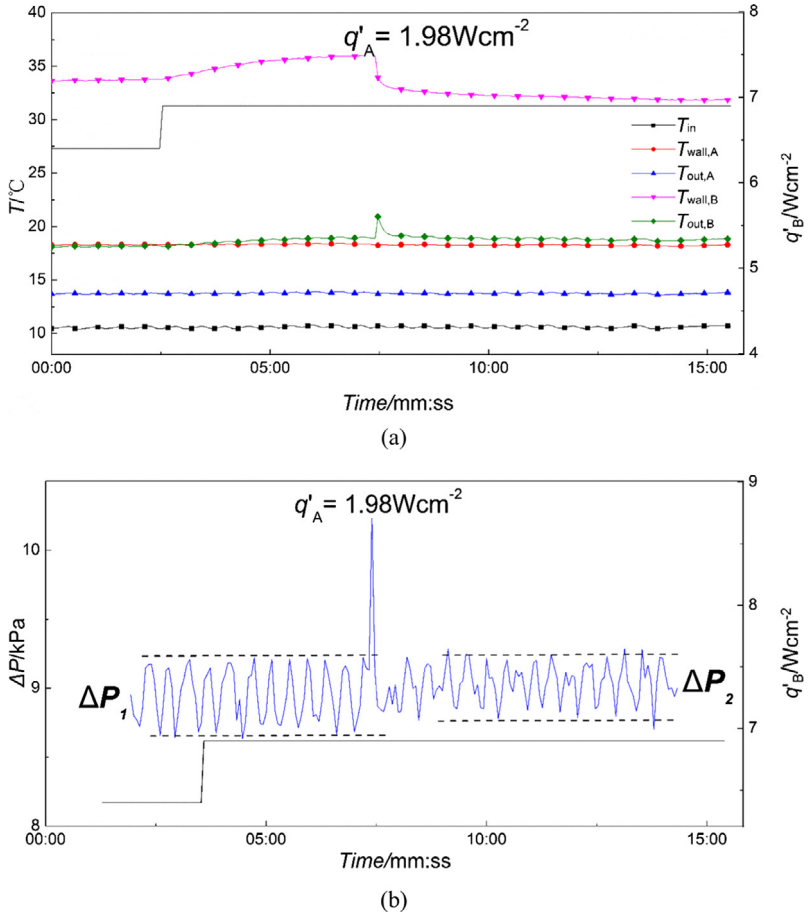

Fig. 14. Heat sink A is in single-phase flow and increase the heat flux of heat sink B at 02:30. The response curves are plotted for: (a) wall temperature and outlet temperature; (b) pressure drop.

For the case that heat sink A is in subcooled flow boiling ($q''_A = 5.93\ \mathrm{W/cm^2}$) in Fig. 12, the bottom surface temperature of heat sink B is lower than that of the single heat sink. This is due to larger flow resistance caused by bubbles generated in heat sink A, and more working fluid flows through the heat sink B while taking away lots of heat. Note that the onset of nucleate boiling (ONB) in heat sink B is delayed, and the outlet temperature of it is reduced.

There is no computational model available for the same conditions as the present work. Therefore, a steady-state mathematical model has been established based on the functions of single heat sink, for the purpose of describing the steady-state characteristics for parallel microchannel heat sinks included in a cooling system with multi-heat source. The mathematical model is shown as follows.

The pressure drop between the inlet and outlet of each heat sink is equal, and it can be written as

$$\Delta P_A = \Delta P_B \tag{14}$$

The total flux rate of two parallel heat sinks is stable at a constant value, and it can be expressed as

$$G_A + G_B = G \tag{15}$$

The pressure drops in single-phase convective flow and subcooled flow boiling are determined respectively by

$$\Delta P_{con} = f_{l,\Delta P}(Re) \tag{16}$$

$$\Delta P_{sub} = f_{v,\Delta P}(Re, Qr) \tag{17}$$

where ΔP_{con} and ΔP_{sub} are obtained from Eqs. (10) and (13).

For the given heating power and total flux rate, the microchannel heat sink bottom surface temperature T_{wall} can be calculated by solving the Eqs. (14) and (15).

When the parallel microchannel heat sinks are both in single-phase flow, the flux and the Reynolds number of each heat sink is equal, and the heat transfer coefficient h can be computed by Eq. (6).

When one of the microchannel heat sinks is in single-phase flow, the other is in subcooled boiling (assuming heat sink A is the former one, heat sink B is the other), the equation can be written as

$$f_{l,\Delta P}(Re_A) = f_{v,\Delta P}(Re_B, Qr_B) \tag{18}$$

When the microchannel heat sinks are in the state of subcooled boiling, the equation is

$$f_{l,\Delta P}(Re_A, Qr_A) = f_{v,\Delta P}(Re_B, Qr_B) \tag{19}$$

In order to verify the reliability of the proposed mathematical model, the bottom surface temperature of heat sinks A and B ($T_{wall,A}$ and $T_{wall,B}$) calculated by above correlations are compared with the present measured data, and the results are given in Fig. 13. For the case in Fig. 13(a), heat sink A is in single-phase flow ($q''_A = 1.98\ \mathrm{W/cm^2}$), and the internal flow of heat sink B changes from single phase into two phase with the gradually increasing

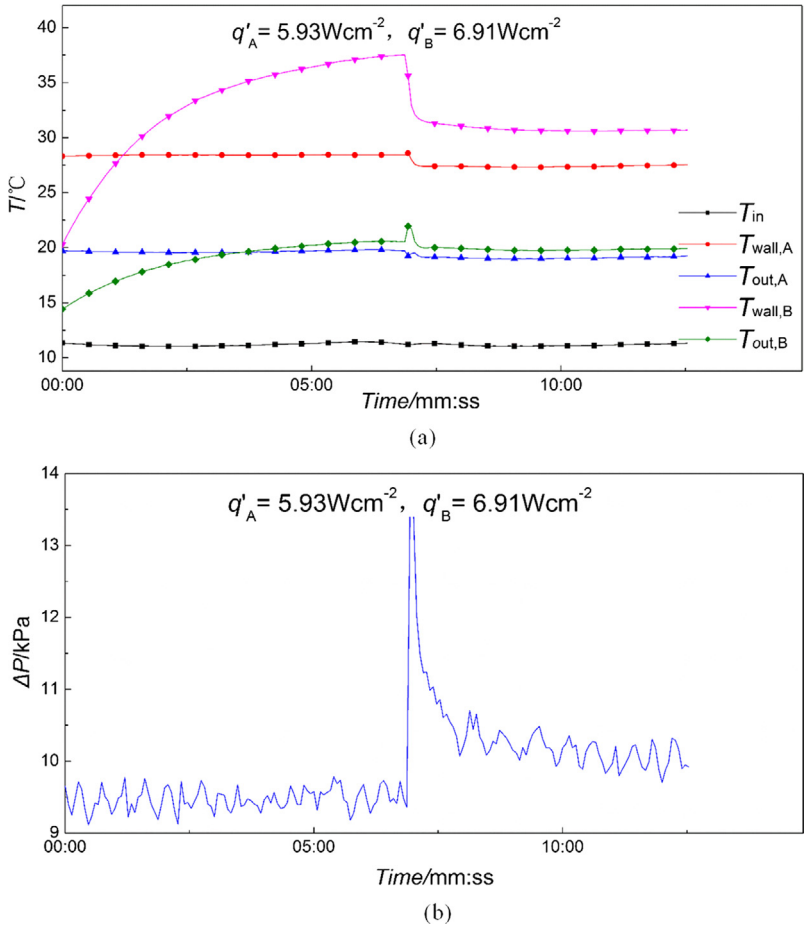

Fig. 15. Heat sink A is in subcooled flow boiling and increase the heat flux of heat sink B at 02:30. The response curves are plotted for: (a) wall temperature and outlet temperature; (b) pressure drop.

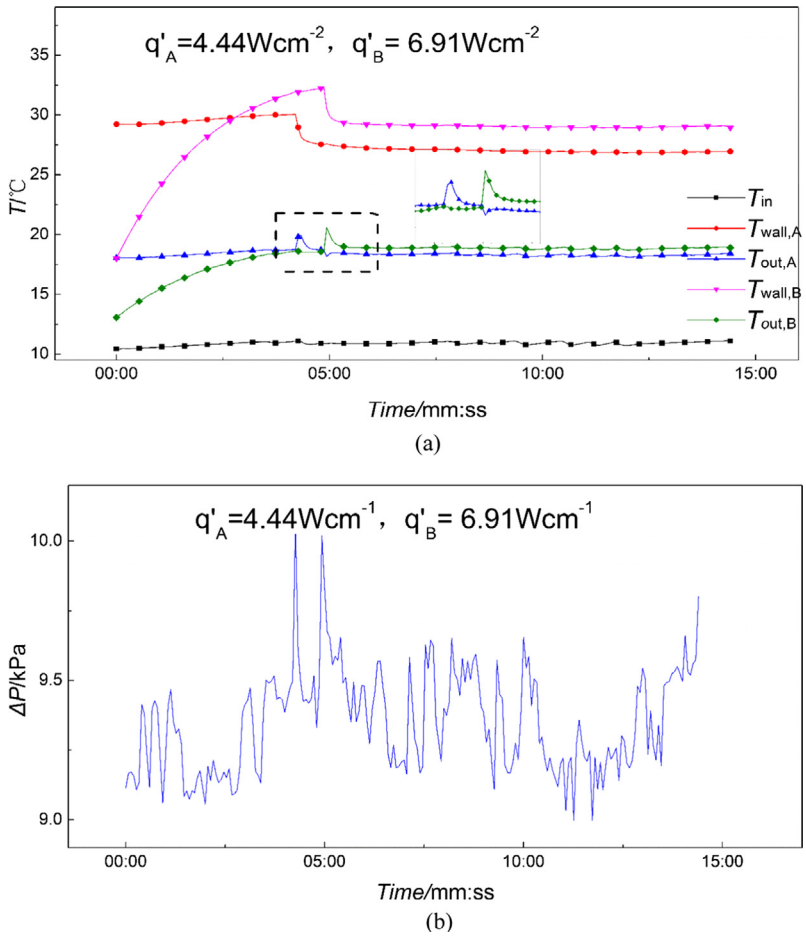

Fig. 16. Heat sink A has been operated under the heating power close to that of the ONB, and then increase the heat flux of heat sink B to 6.91 W/cm^2. The response curves are plotted for: (a) wall temperature and outlet temperature; (b) pressure drop.

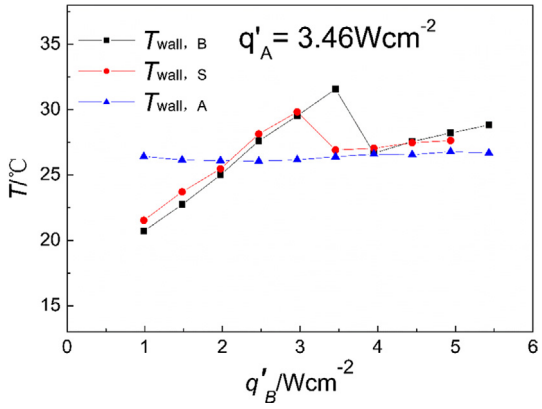

Fig. 17. Comparisons of tandem heat sinks with the single heat sink in terms of steady-state performance.

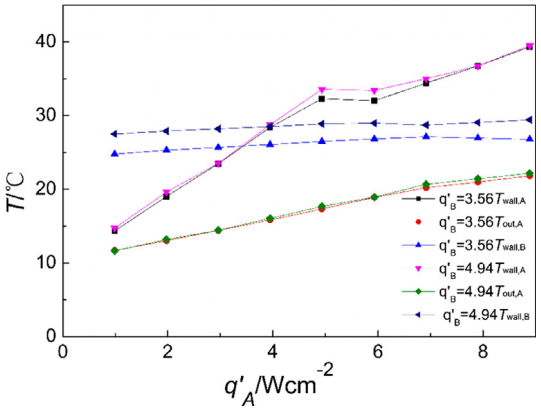

Fig. 18. Variations of $T_{wall,A}$, $T_{out,A}$ and $T_{wall,B}$ with imposed heat flux of heat sink A, for two different states within heat sink B.

heating power. The difference of $T_{wall,A}$ and $T_{wall,B}$ between experiments and correlations is within 15%. While the heat sink A is in subcooled flow boiling ($q''_A = 5.93$ W/cm^2), the variation trends of $T_{wall,A}$ and $T_{wall,B}$ with the heating power of heat sink B are the same in both experiments and correlations, and the maximum error between them is less than 20%, as shown in Fig. 13(b). The results indicate that the proposed correlations are in good agreement with the experimental data.

The dynamic performance of microchannel heat sinks in parallel is exemplified. When the fluid within heat sink A is in single-phase flow ($q''_A = 1.98$ W/cm^2) and increase the heat flux of heat sink B to 6.91 W/cm^2 at 02:30, the bottom surface temperature, outlet temperature and pressure drop of heat sink A, B change accordingly. Fig. 14 shows the response curves of above operating parameters. It should mentioned that the area of heat source used in this experiment was one order of magnitude bigger than that of

common CPUs. Even though the applied heat 6.91 W/cm^2 was not high enough, the actual heat dissipation of the heat sink satisfied the requirement of CPU cooling greatly. Note that phase change occurs in the heat sink B at about 07:30, and the dynamic characteristic of temperature in Fig. 14(a) is basically the same as that of the single heat sink: the fluid near the heated surface absorbs a large amount of heat to generate bubbles. After bubbles lifting off the heated surface, the fluid around there quickly occupies the original location of bubbles and scours the heated surface, resulting in quenching heat flux and that's why the bottom surface temperature plunged. However, the initial bubbles detach into the subcooled bulk liquid flow and just condense slightly because of large diameter, leading to the leap of the outlet temperature. In terms of pressure drop in Fig. 14(b), $\Delta P_1 = 0.58$ kPa and $\Delta P_2 = 0.47$ kPa. ΔP_1 comes from the interaction between the pump head and mass flux, caused by the tiny disturbance in pipeline before the phase transition. The pressure fluctuations in single-phase flow are stable with the consistent frequency. Once the phase change occurs in heat sink B, the bubbles expansion results in the acceleration of downstream fluid and the increase of flow resistance. It also leads to more fluid flow through the heat sink A with larger velocity. The accelerations of the fluid in each heat sink are superposed in parallel outlet, resulting in ΔP_2 less than ΔP_1.

When the fluid within heat sink A is in subcooled flow boiling ($q''_A = 5.93$ W/cm^2), Fig. 15 presents the response curves for the bottom surface temperature, outlet temperature and pressure drop of heat sink A, B after increasing q''_B to 6.91 W/cm^2 at 02:30. The bottom surface temperature of heat sink B, $T_{wall,B}$ gradually rises at the beginning and drops sharply at around 07:20, indicating the generation of subcooled flow boiling. After the phase change occurring in heat sink B, the pressure drop of it increases rapidly, resulting in the rise of flow rate of heat sink A and the reduction in $T_{wall,A}$ and $T_{out,A}$ at almost the same time. Besides, the flow rate of heat sink B decreases within a short time, bringing about more intense phase change and exacerbating uneven flow distribution. Thus it takes longer time for the system to stabilize, about 1 min.

Fig. 16 shows the response curves for the bottom surface temperature, outlet temperature and pressure drop of heat sink A, B respectively, after q''_B up to 6.91 W/cm^2, while the heat sink A has been operated for a period of time under the heating power close to that of the ONB. As the bottom surface temperature of heat sink B, $T_{wall,B}$ increase, phase change occurs in the interior of heat sink A, and then $T_{wall,A}$ drops rapidly, $T_{out,A}$ jumps. The decrease of $T_{wall,B}$ and $T_{out,B}$ is not obvious, because the temperature of heat sink B is still rising at the moment. After the subcooled boiling in heat sink A comes to stabilization, the phase transition takes place in heat sink B, and the change laws are consistent with the above. Due to the fact that phase transitions occur in heat sinks A and B in turn, the pressure drop also leaps successively. Even when the system is stable, the fluctuations and the oscillation frequency of pressure drop are chaotic, indicating the complex mutual influences between two heat sinks in phase change.

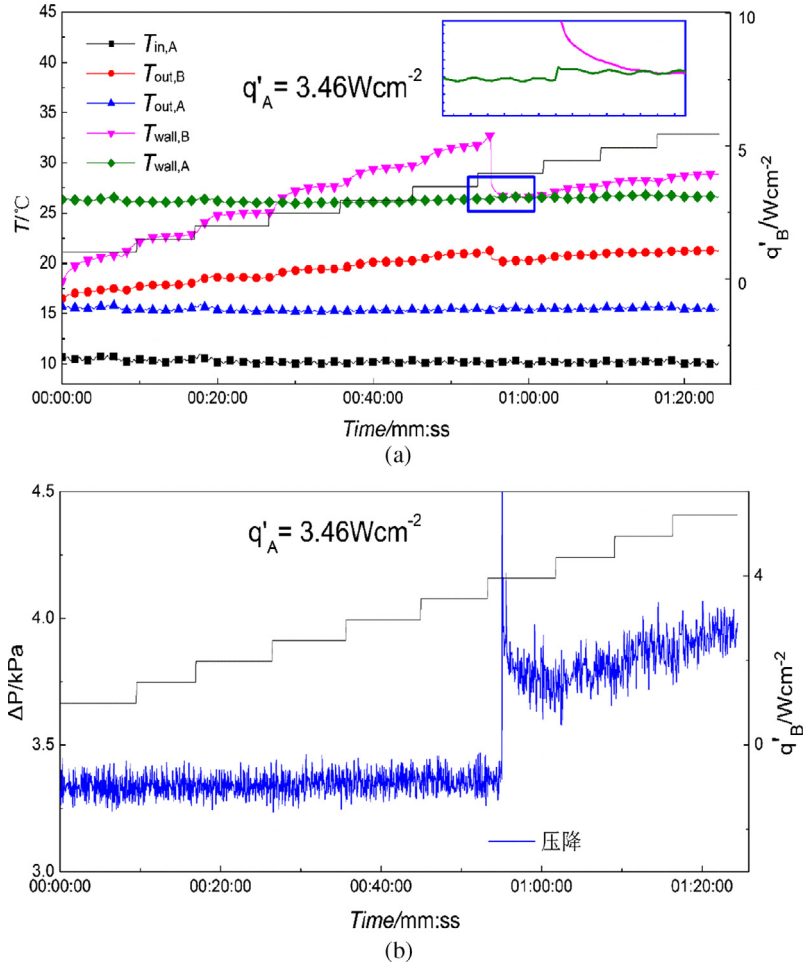

Fig. 19. In the initial state, heat sink A is in subcooled flow boiling and increase the heat flux of heat sink B. The response curves are plotted for: (a) inlet, outlet temperature and bottom surface temperature; (b) pressure drop.

4.2. Experimental results of tandem heat sinks

To study the steady-state performance of heat sink in series, the bottom surface temperature of heat sinks A and B are to be presented in terms of their variations with the imposed heat flux of heat sink B, for heat sink A is in single-phase convective heat transfer ($q''_A = 3.46\ W/cm^2$), and they are compared with the single heat sink under the same operating conditions, as Fig. 17 shows. With the heat flux of heat sink B increasing, the bottom surface temperature of heat sink A, $T_{wall,A}$ changes insignificantly. The results indicate that the downstream effects on the upstream are weak during the steady-state condition. Noted that before q''_B reaching to 3.0 W/cm^2, the heat sink B and the single heat sink are both in single-phase flow, the bottom surface temperature of heat sink B, $T_{wall,B}$ is a bit lower than that of the single heat sink, $T_{wall,S}$. The reason for this phenomenon is that the heat transfer coefficient of heat sink B is slightly increased due to the flow rate fluctuation of the outlet working fluid caused by the density change of the fluid in the upstream. Once the state of the heat sink B and single heat sink transforming into the subcooled boiling, there is no significant difference between $T_{wall,B}$ and $T_{wall,S}$.

Fig. 18 shows the variations of $T_{wall,A}$, $T_{out,A}$ and $T_{wall,B}$ with imposed heat flux of heat sink A, for two different states of heat sink B, single-phase flow and subcooled flow boiling respectively. Under the two states of heat sink B, the curves of $T_{wall,A}$, $T_{out,A}$ are almost coincident with each other, indicating again that the downstream exhibits negligible effects on the upstream during the steady-state condition. The inlet temperature of heat sink B, $T_{out,A}$ gradually increased with the increasing heat flux of heat sink A, resulting in heat sink B easier to enter the saturated boiling. Therefore, it's observed that $T_{wall,B}$ changes gently.

For the purpose of investigating the dynamic performance of the heat sinks in series, Fig. 19 presents the variations of inlet, outlet, and bottom surface temperature of heat sinks A, B with increasing imposed heat flux of heat sink B, when the fluid within heat sink A is in single-phase flow. The change curve of pressure drop of the test section is also illustrated. It's evident that $T_{in,A}$, $T_{out,A}$ and $T_{wall,A}$ are stabilized at a certain value except for the moment phase change occurs in heat sink B. When the fluid within heat sink B enters into subcooled flow boiling, $T_{out,A}$ and $T_{wall,A}$ jump by 0.5 °C and 0.1 °C respectively. The reason accounting for this is that the pressure drop of heat sink B increases suddenly, leading to the decrease of flow rate of heat sink A. It is worth mentioning that the heat flux of heat sink B has no significant effect on the performance of heat sink A.

As Fig. 20 shows, the inlet, outlet, and bottom surface temperature of heat sinks A, B and the pressure drop of the test section vary with the imposed heat flux of heat sink A, for the condition that the fluid within heat sink B is in single-phase flow at the initial state. The results show the phase transition occurs in heat sink A at around 01:12:00, with ΔP increasing rapidly. It is reasonable to speculate that the existence of heat sink B has no effects on reducing the pressure drop of system. Meanwhile, $T_{out,A}$, $T_{out,B}$ and $T_{wall,B}$ decrease by about 2.5 °C. The reason is that the pressure drops of

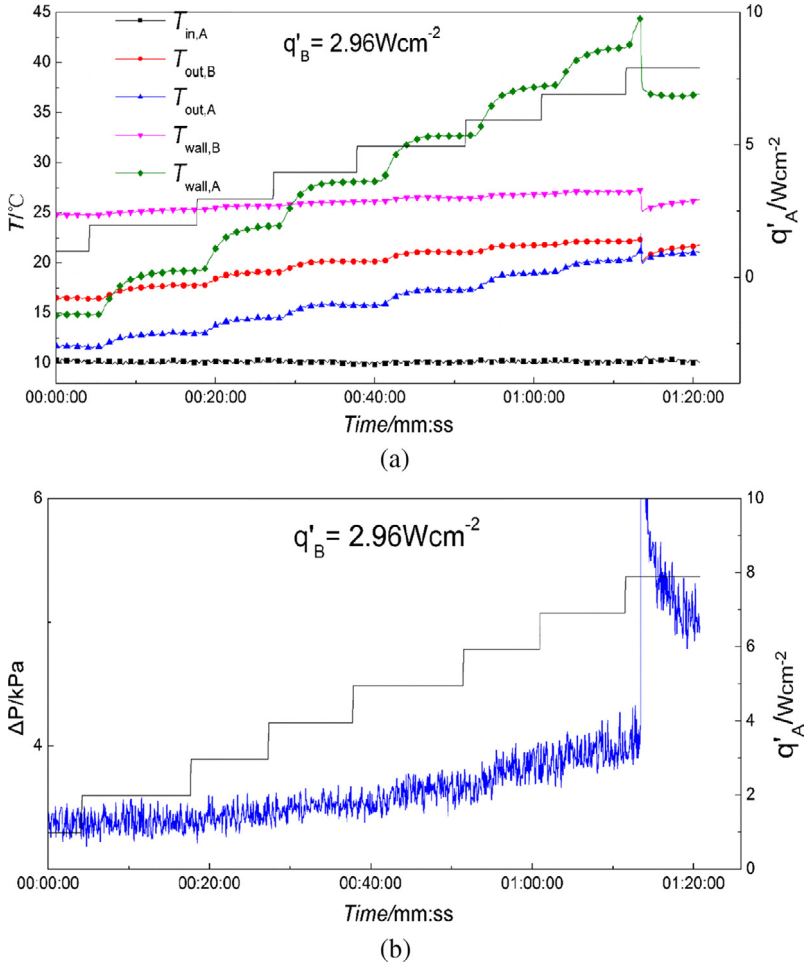

Fig. 20. In the initial state, heat sink B is in single-phase flow and increase the heat flux of heat sink A. The response curves are plotted for: (a) inlet, outlet temperature and bottom surface temperature; (b) pressure drop.

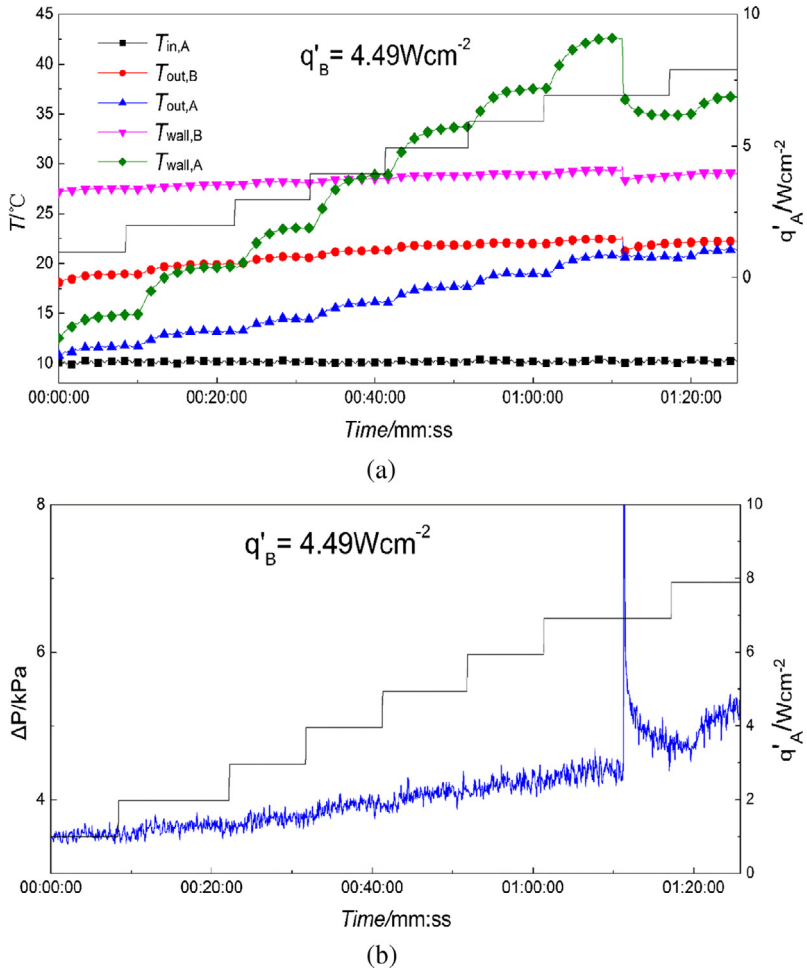

Fig. 21. In the initial state, heat sink B is in subcooled flow boiling and increase the heat flux of heat sink A. The response curves are plotted for: (a) inlet, outlet temperature and bottom surface temperature; (b) pressure drop.

heat sink A increase during the phase transformation, resulting in the fluid of heat sink B accelerating and scouring the wall intensively. When the flow is stable, the scouring effect is weakened and the temperature gradually recovers.

For the initial flow condition of heat sink B is subcooled flow boiling, the experiments investigate the effects of imposed heat flux of heat sink A on the temperature and pressure drop of the micro-channel heat sinks, as shown in Fig. 21. Similar to the Fig. 20, the influence of heat sink A on heat sink B is mainly to change the inlet temperature and working fluid velocity of it, resulting in the decrease of $T_{out,B}$ and $T_{wall,B}$.

5. Conclusions

The microchannel cooling system consisting of two heat sinks is designed for dissipating high heat flux from multi-heat heat sources efficiently. The heat sinks are connected in parallel or in series and the mutual influences between them are further investigated from both dynamic and stable aspects. The experimental data shows that:

(1) For parallel connection, the interactions are mainly manifested in the case of two heat sinks different in heat transfer forms. Pressure drop of the heat sink in subcooled boiling changes and eventually results in uneven mass flux distribution, where flow rate of the above heat sink becomes less than 0.4 L/min, and that of the heat sink in single-phase convective flow is more than 0.4 L/min. The aforementioned phenomenon is obvious in both steady and dynamic states.

(2) For tandem connection, temperature of upstream heat sink remains constant except for the moment phase change occurs in downstream heat sink. Under that circumstance, rapid change of the downstream pressure drop impacts the upstream temperature dynamically with outlet and wall temperature of the upstream heat sink jumping by 0.5 °C and 0.1 °C respectively. The influences are weak as flow becomes stable, indicating that downstream has little effects on the upstream. But phase transition of upstream heat sink affects heat transfer properties and flow instability of the downstream one more intensely, with inlet, outlet and wall temperature of the downstream one decreasing by 2.5 °C.

(3) Based on experimental data, correlation equations for heat transfer coefficients and friction factors of single heat sink in single-phase convective flow and subcooled flow boiling have been proposed to provide acceptable predictions in both accuracy and trend, evidenced by mean absolute errors less than 8%.

(4) The study has proved different connections of the microchannel heat sinks result in mutual heat effects between the multi-heat sources. A steady-state mathematical model is established to describe the steady-state characteristics for parallel heat sinks. It is important to establish

more accurate theoretical models accounting for the interactions between the heat sinks. The width and depth of microchannels are also significant factors for heat transfer performance, and these factors will be taken into consideration in future in-depth study.

(5) The microchannel heat sinks cooling system proposed has various advantages of compact structure, simple connection, cost-saving, easy-maintenance, reliable operation and so on. The experiments are of great significance and reference value for the heat dissipation problem of multi-heat sources and high heat flux electronic devices in practical engineering applications.

Acknowledgements

The work is supported by the National Key Basic Research Program of China (973 Program) (2013CB228302) and the National Natural Science Foundation of China (51376069).

References

[1] Tuckerman DB, Pease R. High-performance heat sinking for VLSI. IEEE Electron Device Lett 1981;2(5):126–9.
[2] Shen S, Xu JL, Zhou JJ, Chen Y. Flow and heat transfer in microchannels with rough wall surface. Energy Convers Manage 2006;47(11–12):1311–25.
[3] Yun R, Heo JH, Kim Y. Evaporative heat transfer and pressure drop of R410A in microchannels. Int J Refrig 2006;29(1):92–100.
[4] Yan Y-Y, Lin T-F. Evaporation heat transfer and pressure drop of refrigerant R-134a in a small pipe. Int J Heat Mass Transf 1998;41(24):4183–94.
[5] Saitoh S, Daiguji H, Hihara E. Effect of tube diameter on boiling heat transfer of R-134a in horizontal small-diameter tubes. Int J Heat Mass Transf 2005;48(23–24):4973–84.
[6] Qu W, Mudawar I. Measurement and correlation of critical heat flux in two-phase micro-channel heat sinks. Int J Heat Mass Transf 2004;47(10):2045–59.
[7] Lie Y, Su F, Lai R, Lin T. Experimental study of evaporation heat transfer characteristics of refrigerants R-134a and R-407C in horizontal small tubes. Int J Heat Mass Transf 2006;49(1):207–18.
[8] Madhour Y, Olivier J, Costa-Patry E, Paredes S, Michel B, Thome JR. Flow boiling of R134a in a multi-microchannel heat sink with hotspot heaters for energy-efficient microelectronic CPU cooling applications. IEEE Trans Compon Pack Manuf Technol 2011;1(6):873–83.
[9] do Nascimento FJ, Leão HLSL, Ribatski G. An experimental study on flow boiling heat transfer of R134a in a microchannel-based heat sink. Exp Therm Fluid Sci 2013;45:117–27.
[10] Xu J, Zhou J, Gan Y. Static and dynamic flow instability of a parallel microchannel heat sink at high heat fluxes. Energy Convers Manage 2005;46(2):313–34.
[11] Thiangtham P, Keepaiboon C, Kiatpachai P, Asirvatham LG, Mahian O, Dalkilic AS, et al. An experimental study on two-phase flow patterns and heat transfer characteristics during boiling of R134a flowing through a multi-microchannel heat sink. Int J Heat Mass Transf 2016;98:390–400.
[12] Tran TN, Wambsganss MW, France DM. Small circular- and rectangular-channel boiling with two refrigerants. Int J Multiph Flow 1996;22(3):485–98.
[13] Owhaib W, Martín-Callizo C, Palm B. Evaporative heat transfer in vertical circular microchannels. Appl Therm Eng 2004;24(8):1241–53.
[14] Bao Z, Fletcher D, Haynes B. Flow boiling heat transfer of Freon R11 and HCFC123 in narrow passages. Int J Heat Mass Transf 2000;43(18):3347–58.
[15] Chang KH, Pan C. Two-phase flow instability for boiling in a microchannel heat sink. Int J Heat Mass Transf 2007;50(11–12):2078–88.
[16] Dong T, Yang Z, Bi Q, Zhang Y. Freon R141b flow boiling in silicon microchannel heat sinks: experimental investigation. Heat Mass Transf 2008;44(3):315–24.
[17] Bigham S, Moghaddam S. Microscale study of mechanisms of heat transfer during flow boiling in a microchannel. Int J Heat Mass Transf 2015;88:111–21.
[18] Huang H, Borhani N, Thome JR. Experimental investigation on flow boiling pressure drop and heat transfer of R1233zd(E) in a multi-microchannel evaporator. Int J Heat Mass Transf 2016;98:596–610.
[19] Lee S, Mudawar I. Investigation of flow boiling in large micro-channel heat exchangers in a refrigeration loop for space applications. Int J Heat Mass Transf 2016;97:110–29.
[20] Markal B, Aydin O, Avci M. An experimental investigation of saturated flow boiling heat transfer and pressure drop in square microchannels. Int J Refrig 2016;65:1–11.
[21] Mauro AW, Thome JR, Toto D, Vanoli GP. Saturated critical heat flux in a multi-microchannel heat sink fed by a split flow system. Exp Therm Fluid Sci 2010;34(1):81–92.
[22] Wu JM, Zhao JY, Tseng KJ. Parametric study on the performance of double-layered microchannels heat sink. Energy Convers Manage 2014;80:550–60.
[23] Deng D, Wan W, Shao H, Tang Y, Feng J, Zeng J. Effects of operation parameters on flow boiling characteristics of heat sink cooling systems with reentrant porous microchannels. Energy Convers Manage 2015;96:340–51.
[24] Deng D, Wan W, Tang Y, Wan Z, Liang D. Experimental investigations on flow boiling performance of reentrant and rectangular microchannels – a comparative study. Int J Heat Mass Transf 2015;82:435–46.
[25] Dehghan M, Valipour MS, Saedodin S. Microchannels enhanced by porous materials: heat transfer enhancement or pressure drop increment? Energy Convers Manage 2016;110:22–32.
[26] Zhang S, Tang Y, Zeng J, Yuan W, Chen J, Chen C. Pool boiling heat transfer enhancement by porous interconnected microchannel nets at different liquid subcooling. Appl Therm Eng 2016;93:1135–44.
[27] Xia G, Ma D, Zhai Y, Li Y, Liu R, Du M. Experimental and numerical study of fluid flow and heat transfer characteristics in microchannel heat sink with complex structure. Energy Convers Manage 2015;105:848–57.
[28] Law M, Lee P-S, Balasubramanian K. Experimental investigation of flow boiling heat transfer in novel oblique-finned microchannels. Int J Heat Mass Transf 2014;76:419–31.
[29] Law M, Lee P-S. A comparative study of experimental flow boiling heat transfer and pressure characteristics in straight- and oblique-finned microchannels. Int J Heat Mass Transf 2015;85:797–810.
[30] Marquardt DW. An algorithm for least-squares estimation of nonlinear parameters. J Soc Ind Appl Math 1963;11(2):431–41.